

MIT Open Access Articles

Optoelectronic Properties in Monolayers of Hybridized Graphene and Hexagonal Boron Nitride

The MIT Faculty has made this article openly available. **Please share** how this access benefits you. Your story matters.

Citation: Bernardi, Marco, Maurizia Palummo, and Jeffrey Grossman. "Optoelectronic Properties in Monolayers of Hybridized Graphene and Hexagonal Boron Nitride." *Physical Review Letters* 108.22 (2012). © 2012 American Physical Society

As Published: <http://dx.doi.org/10.1103/PhysRevLett.108.226805>

Publisher: American Physical Society

Persistent URL: <http://hdl.handle.net/1721.1/72379>

Version: Final published version: final published article, as it appeared in a journal, conference proceedings, or other formally published context

Terms of Use: Article is made available in accordance with the publisher's policy and may be subject to US copyright law. Please refer to the publisher's site for terms of use.



Optoelectronic Properties in Monolayers of Hybridized Graphene and Hexagonal Boron Nitride

Marco Bernardi,¹ Maurizia Palumbo,² and Jeffrey C. Grossman^{1,*}

¹*Department of Materials Science and Engineering, Massachusetts Institute of Technology, 77 Massachusetts Avenue, Cambridge, Massachusetts 02139-4307, USA*

²*Dipartimento di Fisica, Università di Roma Tor Vergata, NAST, and European Theoretical Spectroscopy Facility (ETSF), Via della Ricerca Scientifica 1, 00133 Roma, Italy*

(Received 2 February 2012; published 1 June 2012)

We explain the nature of the electronic energy gap and optical absorption spectrum of carbon–boron–nitride (CBN) monolayers using density functional theory, *GW* and Bethe–Salpeter calculations. The band structure and the optical absorption are regulated by the C domain size rather than the composition (as customary for bulk semiconductor alloys). The C and BN quasiparticle states lie at separate energy for C and BN, with little mixing for energies near the band edge where states are chiefly C in character. The resulting optical absorption spectra show two distinct peaks whose energy and relative intensity vary with composition in agreement with the experiment. The monolayers present strongly bound excitons localized within the C domains, with binding energies of the order of 0.5–1.5 eV dependent on the C domain size. The optoelectronic properties result from the overall monolayer band structure, and cannot be understood as a superposition of the properties of bulklike C and BN domains.

DOI: 10.1103/PhysRevLett.108.226805

PACS numbers: 73.22.-f, 71.35.-y, 78.67.-n

Recently, two-dimensional (2D) materials with a finite band gap and high carrier mobility have been synthesized and characterized, chiefly in view of their use in optoelectronic devices [1,2]. Among these, monolayers of hybridized carbon and boron nitride (CBN) present highly appealing optoelectronic properties due to their tunable electronic energy gap, physically deriving from the large energy gap difference between pure hexagonal BN (*h*-BN, energy gap $E_g > 5.0$ eV) and graphene, a semimetal with zero energy gap [3]. The C and BN phases are immiscible in 2D, leading to phase separation in the sheet with formation of distinct C and BN domains [1].

The optical absorption spectrum of CBN measured in the recent work from Li *et al.* [1] shows two main absorption edges located (using Tauc’s extrapolation procedure [4]) at around 1.6 and 4.5 eV for a sample with 65% C content, while for a higher C concentration such absorption peaks were shifted to lower energies. These two features were attributed to the existence of C and *h*-BN domains large enough to resume their individual band gap identities, rather than behave as a CBN alloy [1].

The electronic band gap of the CBN monolayer has been calculated for different C and BN domain geometries including quantum dots and superlattices, using tight-binding and density functional theory (DFT) calculations [5–11]. These geometries can only approximate on a local scale the experimental structure of disordered C and BN domains synthesized in Ref. [1].

For quantum dot geometries, the band gap tunability arises due to confinement in both dimensions [8], but DFT level calculations were only applied to limited domain sizes up to approximately 1 nm, well below the experimental value. CBN 2D superlattices, modeled as

alternating C and BN stripe domains within the monolayer, can provide band gap values closer to experiment due to lack of confinement in both dimensions. Previous results have addressed the band gap tunability as a function of composition [6] rather than domain size, or the differences between hydrogenated C nanoribbons and C nanoribbons formed within CBN superlattices [5,12]. However, a detailed interpretation of the experimental optical absorption spectrum in Ref. [1] for disordered CBN and its connection to the calculated band structure has been lacking.

Here we shed light on the optoelectronic properties of CBN monolayers and show that the double optical peak measured by Ci *et al.* [1] is inherently related to the overall band structure of the CBN system. Such excitation peaks are not due to large C and BN domains, but rather to the near absence of the mixing of C and BN states at the valence band maximum (VBM) and conduction band minimum (CBM). This generates two distinct sets of optical transitions: low energy transitions between C states near the band gap resulting in bound bright excitons localized within the C domains, and higher energy transitions from states that are mostly BN-like in character and lie deeper within the conduction and valence bands.

In addition, we demonstrate that C domain size rather than monolayer chemical composition regulates the CBN band structure and optical absorption. This is in contrast with the well-known behavior of bulk semiconductor alloys whose energy gap varies continuously with the concentration of the composing elements [13]. We also find large corrections to the DFT band gaps using *GW* calculations and strongly bound excitons, both effects contributing to an optical absorption spectrum similar to

the random-phase approximation (RPA) DFT spectrum due to large error compensations in the latter.

We carried out *ab initio* DFT calculations using the QUANTUM ESPRESSO code [14] separately on CBN superlattices with armchair and zigzag edges. An orthorhombic unit cell was adopted for the armchair structure and a hexagonal unit cell was used for the zigzag case (Fig. 1). A vacuum spacing of 15 Å was used in the direction perpendicular to the sheet to avoid spurious interaction with the image system. We employed a total number of 8 or 16 C and BN atom rows in the unit cell (Fig. 1) in distinct sets of calculations. In this way, electronic structure data are available for a given composition for two different values of C domain sizes. The Perdew-Burke-Ernzerhof exchange correlation functional [15] is adopted and ultrasoft pseudopotentials [16] are used to describe the core electrons. A kinetic energy cutoff of 35 Ry was used for the plane-wave basis set and of 200 Ry for the charge density. Converged Monkhorst-Pack \vec{k} -point grids [17] of $3 \times 3 \times 1$ and $15 \times 5 \times 1$ were used for the zigzag and armchair cases, respectively.

The *GW* and Bethe-Salpeter equation (BSE) calculations [18] were performed on three armchair cases [19] with different C concentrations using the Yambo code [20,21]. Briefly, a plasmon-pole model was adopted for the dielectric function and cutoff energies of 35 and 5 Ry were used, respectively, for the exchange and correlation part of the self-energy; the Coulomb interaction was truncated in the direction perpendicular to the sheet to avoid spurious interactions with the image system. The *GW* calculations were performed without self-consistency in

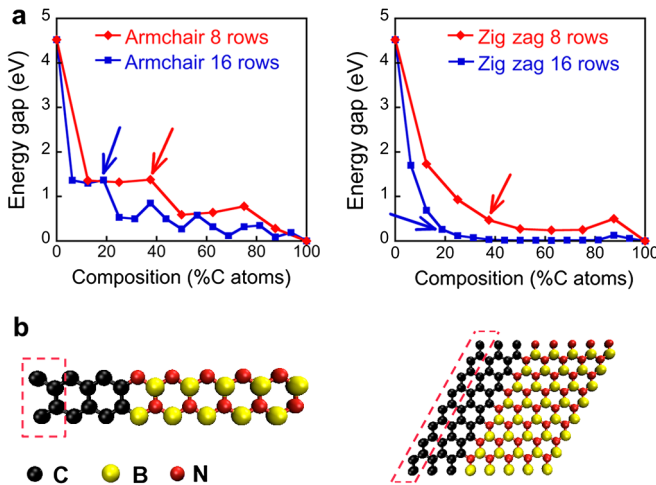


FIG. 1 (color online). (a) Kohn-Sham band gap calculated using DFT for CBN superlattices with armchair (left) and zigzag (right) edge. Starting from pure BN (zero percent C), each consecutive point for increasing C concentrations corresponds to the addition of a C row to the structure. (b) Unit cells employed in the 8-rows calculations for the armchair (left) and zigzag (right) cases. The parts referred to as “one row” in the text are shown in dashed boxes.

the Green’s function and the screened Coulomb interaction (G_0W_0 approximation scheme). A total number of 300 bands (> 150 empty bands) was used, together with a converged \vec{k} -point grid of $16 \times 6 \times 1$. Both DFT and *GW* levels of theory were employed in combination with RPA or BSE calculations to compute the optical absorption spectra.

Figure 1(a) shows the evolution of the DFT band gap as a function of C concentration for armchair and zigzag superlattices with a total of 8 and 16 atom rows in the simulation cell. As the C concentration is increased, the energy gap decreases from 4.6 eV for pure *h*-BN to zero for pure graphene, with a sudden drop to < 2.0 eV following the introduction of a single C row, as observed in previous work [5]. For a given composition, the two cases with different number of atom rows give different band gap values; the same band gap value for the two systems is found when comparing superlattices with the same number of C rows (and thus same C domain size). For example, the arrows in Fig. 1(a) point to structures with three C rows, corresponding to different concentrations for systems with a total of 8 and 16 rows in the unit cell, and yet showing the same energy gap to within 0.1 eV. This behavior is observed for all such pairs of structures with the same number of C rows, both for the armchair and the zigzag cases.

A more detailed analysis of the DFT electronic structure is presented in Fig. 2, where the CBN systems are labeled $C_x(\text{BN})_{(8-x)}$ for superlattices with x carbon rows out of a total of 8 rows in the unit cell. A direct band gap was found for all the armchair and zigzag systems studied, thus justifying the high optical absorption observed experimentally. In the armchair cases shown here, the band gap closes progressively for increasing C concentrations but the formation of the Dirac cone only occurs when 1–2 residual BN rows are present, as seen by the increasing dispersion in the Y - Γ direction (normal to the domain edge) resulting in the closure of the gap at the equivalent of the K point of the hexagonal lattice [22]. We interpret this behavior as a sign of the incipient delocalization of the VBM and CBM states when the system is close to being a sheet of pure graphene.

The projected density of states (PDOS) shows that for all the compositions studied, the states with energy near the gap are mainly due to C, while states farther in energy from the gap result from the hybridization of C and BN atomic orbitals. The zigzag case shows analogous behavior (see Supplemental Material [23]), with subtle differences in the band gap closing near the pure C composition that occurs through a band-crossing mechanism for the formation of the Dirac cone at the K point, causing the slight bump seen in the band gap values in Fig. 1(a) at large C fractions.

The dependence of the band gap on the C domain size, rather than on the overall CBN layer composition [23], can be regarded as an electronic size effect, whereby the C states near the band gap are confined by an effective

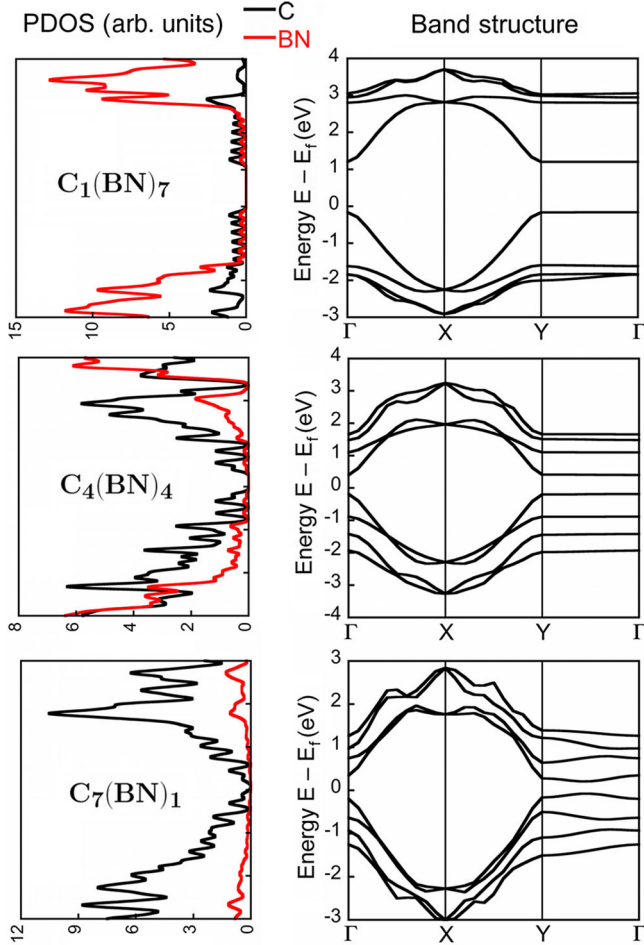


FIG. 2 (color online). PDOS and corresponding band structure plots for three armchair superlattices. The energies are referred to the Fermi energy E_f . The C domain size increases from the top to the bottom panel, and the band gap decreases accordingly. The Dirac cone typical of graphene starts forming for 1-2 residual BN rows, as seen in the bottom panel for the $C_7(\text{BN})_1$ case, where the dispersion along the Y - Γ line culminates in the formation of the Dirac cone. The PDOS shows that the states close in energy to the gap are mainly due to mixing of C valence states with almost no contribution from BN.

quasiparticle barrier within the conduction and valence bands formed by the BN states, as seen by the analysis of the PDOS. Nevertheless, the detail of the edge type and binding at the CBN interface is also relevant to determine the specific value of the gap (and consequently of the optical properties), as shown by the different band gap values for the zigzag and armchair cases.

Next, we analyze the results from the GW and BSE calculations. For the three armchair cases studied with beyond-DFT methods, we found quasiparticle (GW) band gap values significantly higher than the DFT gap (Table I), with corrections in the range of 0.7–1.9 eV. On the other hand, the optical gap (GW -BSE) values were found to be within 0.4 eV of the DFT gaps due to large exciton binding energies in the range of 0.7–1.5 eV

TABLE I. Values of the band gap (in eV) within different approximations for three armchair structures studied with beyond-DFT methods. The exciton binding energy (in eV) is also shown.

Structure	DFT	GW	$GW + \text{BSE}$	Exciton binding energy
$C_1(\text{BN})_7$ (12.5% C)	1.39	3.25	1.80	1.45
$C_4(\text{BN})_4$ (50% C)	0.60	1.72	0.59	1.04
$C_7(\text{BN})_1$ (87.5% C)	0.30	1.04	0.32	0.72

(Table I), inferred from the difference between the quasiparticle (GW) and optical (GW -BSE) gaps.

The DFT-RPA absorption spectra for the armchair [Fig. 3(a)] and zigzag (see Supplemental Material [23]) cases show two absorption peaks resulting from the DFT band structures in Fig. 2, with transitions due to the direct band gap along the Y - Γ direction (low energy absorption onset) and to the direct gap from higher energy states formed at the X point. These two features are retained in the GW -BSE spectrum [Fig. 3(b)] and can be interpreted as the reason for the two absorption peaks observed experimentally in the work of Ci *et al.* [1].

The GW -BSE spectrum contains information about two important physical effects: the opening of the quasiparticle gap due to electron-electron interactions at the GW level of theory, causing by itself an almost rigid blueshift of the absorption spectrum [GW -RPA curve in Fig. 3(b)], and the formation of bound excitonic states resulting in a redshift of the spectrum back to energies similar to the DFT-RPA approximation level, as seen in the GW -BSE spectra in Fig. 3(b). This explains the excellent qualitative agreement of the DFT-RPA optical absorption spectrum seen in Fig. 3(b), due to a compensation of significant errors within DFT.

Consistent with the experiments by Ci *et al.* [1], for increasing C concentrations both absorption peaks are redshifted and their relative intensity varies, thus showing the tunability of the optical properties of the CBN sheet. By comparing with Ref. [1] where systems with over 65% C concentration show an optical gap of 1.5 eV, we infer that such a low energy absorption edge arises from small C domains with at least one dimension of 1–2 nm length. We note, however, that the Tauc's extrapolation procedure [4] used in Ref. [1] can lead to significant errors in the estimation of the absorption onset. Our results suggest that the experimental spectrum should be regarded as formed by the superposition of the spectra shown in Fig. 3 weighted for the different C domain sizes present in the system, justified by the absence of a well-defined low energy peak in the experimental absorption data [1].

The exciton wave function obtained within the BSE framework [Fig. 3(c)] is found to be confined by an effective quasiparticle gap at the CBN interfaces. When the hole

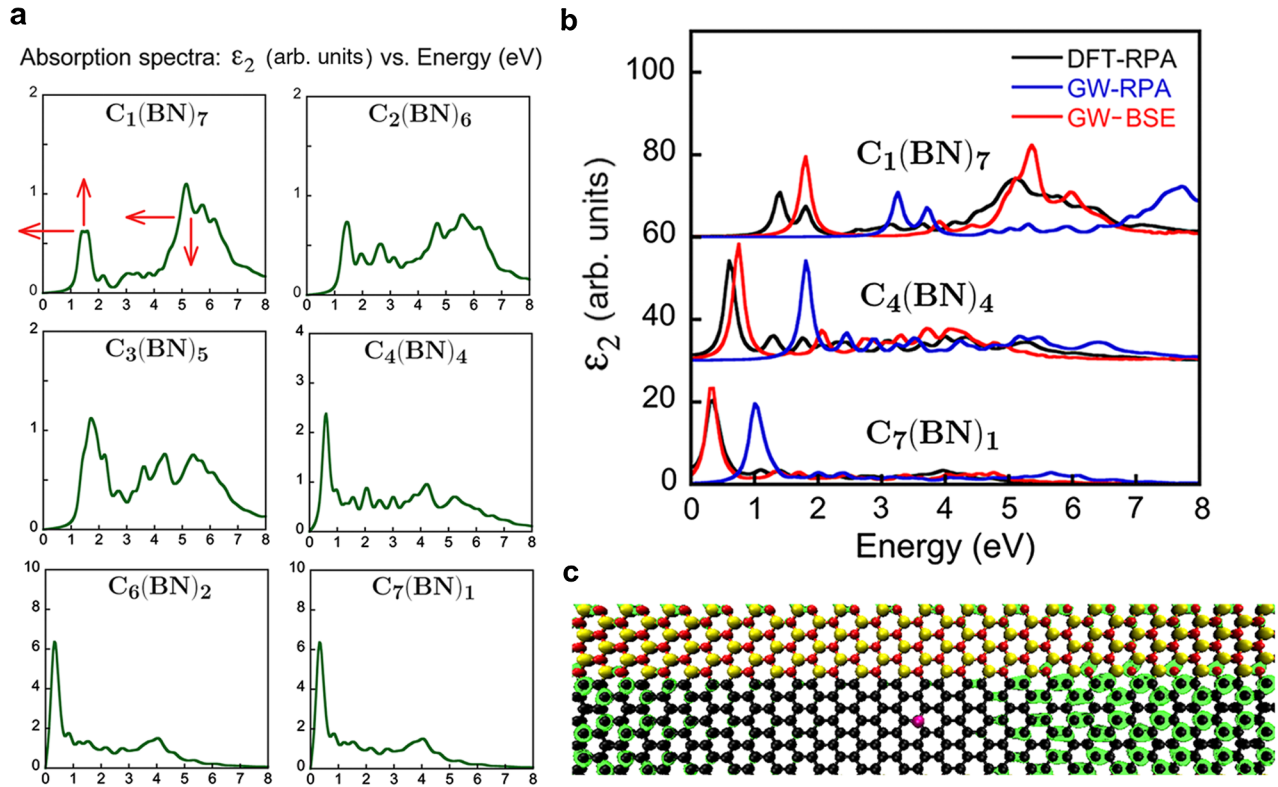


FIG. 3 (color online). (a) Evolution of the DFT-RPA optical absorption (expressed as the imaginary part of the dielectric tensor, ϵ_2) for increasing sizes of the C domain, for the armchair structures with 8 atom rows shown in Fig. 1(a). The two absorption peaks redshift and vary their relative strength for an increasing C domain size as indicated by the arrows. (b) Comparison of absorption spectra for the armchair structures discussed in Table I. The imaginary part of the dielectric tensor (averaged for the three directions) is shown for different levels of approximation including DFT-RPA, GW-RPA, and GW-BSE. (c) Exciton wave function for the $C_4(\text{BN})_4$ armchair superlattice. Shown is the probability density distribution for the electron (isosurface plot, shown in green online) that localizes within the C domain when the hole position is fixed in the middle of the C domain (shown as a magenta spot online). The atoms coloring follows the legend in Fig. 1(b).

is fixed in a given position within the C domain, the electron wave function localizes within the same C domain, which is compatible with the presence of VBM and CBM states with C character, and BN-like states farther in energy from the gap. Such delocalized, yet strongly bound bright excitons are a unique feature of nanoscale systems that has been predicted previously for 1D armchair graphene nanoribbons [24].

In summary, we elucidate the mechanisms underlying the band gap formation and optical processes including absorption and excitons in the CBN monolayer. We find that the energy gap is uniquely regulated by the size of the C domains regardless of the overall system composition, a trend in clear contrast with the behavior of bulk semiconductor alloys. The absorption spectra of CBN monolayers show two main absorption peaks whose strength and position depend on the C domain size, with transitions between the VBM and CBM states contributing to the low energy absorption onset and to the formation of strongly bound excitons within the C domains. Large quasiparticle and excitonic corrections show that DFT calculations are inadequate to predict the experimental behavior of 2D CBN

alloys. The unique dependence of the band gap and absorption spectrum on domain size rather than concentration opens new possibilities for band gap engineering and for optoelectronic and photovoltaic applications distinct from those existing for *h*-BN and graphene. Similar tunable optoelectronic properties and large excitonic effects have been observed recently for MoS_2 monolayers [25,26]. This new family of 2D nanomaterials constitutes a novel playground for optoelectronic and excitonic devices.

M. B. acknowledges funding from Intel through the Intel Ph.D. Fellowship. We wish to thank NERSC for providing computational resources.

*jcg@mit.edu

- [1] L. Ci, L. Song, C. Jin, D. Jariwala, D. Wu, Y. Li, A. Srivastava, Z. F. Wang, K. Storr, L. Balicas, F. Liu, and P. M. Ajayan, *Nature Mater.* **9**, 430 (2010).
- [2] B. Radisavljevic, A. Radenovic, J. Brivio, V. Giacometti, and A. Kis, *Nature Nanotech.* **6**, 147 (2011).
- [3] A. Geim, *Science* **324**, 1530 (2009).

- [4] J. Tauc, R. Grigorovici, and A. Vancu, *Phys. Status Solidi* **15**, 627 (1966).
- [5] G. Seol and J. Guo, *Appl. Phys. Lett.* **98**, 143107 (2011).
- [6] K.-T. Lam, Y. Lu, Y.P. Feng, and G. Liang, *Appl. Phys. Lett.* **98**, 022101 (2011).
- [7] A. K. Manna and S. K. Pati, *J. Phys. Chem. C* **115**, 10842 (2011).
- [8] J. Li and V.B. Shenoy, *Appl. Phys. Lett.* **98**, 013105 (2011).
- [9] A. Y. Liu, R. M. Wentzcovitch, and M. L. Cohen, *Phys. Rev. B* **39**, 1760 (1989).
- [10] J. R. Martins and H. Chacham, *ACS Nano* **5**, 385 (2011).
- [11] X. Blase, J.-C. Charlier, A. D. Vita, and R. Car, *Appl. Phys. A* **68**, 293 (1999).
- [12] Y.-W. Son, M. L. Cohen, and S. G. Louie, *Phys. Rev. Lett.* **97**, 216803 (2006).
- [13] M. Jaros, *Rep. Prog. Phys.* **48**, 1091 (1985).
- [14] P. Giannozzi, S. Baroni, N. Bonini, M. Calandra, R. Car, C. Cavazzoni, D. Ceresoli, G. L. Chiarotti, M. Cococcioni, I. Dabo, A. Dal Corso, S. de Gironcoli, S. Fabris, G. Fratesi, R. Gebauer, U. Gerstmann, C. Gougoussis, A. Kokalj, M. Lazzeri, L. Martin-Samos, *et al.*, *J. Phys. Condens. Matter* **21**, 395502 (2009).
- [15] J. P. Perdew, K. Burke, and M. Ernzerhof, *Phys. Rev. Lett.* **77**, 3865 (1996).
- [16] D. Vanderbilt, *Phys. Rev. B* **41**, 7892 (1990).
- [17] H. J. Monkhorst and J. D. Pack, *Phys. Rev. B* **13**, 5188 (1976).
- [18] G. Onida, L. Reining, and A. Rubio, *Rev. Mod. Phys.* **74**, 601 (2002).
- [19] We calculated the formation energy of the armchair and zigzag type edges and inferred a ratio of 2.5 between the thermal equilibrium length of the armchair and zigzag domain edges at intermediate compositions and room temperature. This justifies our more accurate study of the optical properties and band gap for the armchair edge type as it is expected to contribute more significantly to the experimental results observed in [1].
- [20] A. Marini, C. Hogan, M. Gruning, and D. Varsano, *Comput. Phys. Commun.* **180**, 1392 (2009).
- [21] For the calculations performed with the Yambo code, the ground state Kohn-Sham wave functions and eigenvalues were obtained using an LDA exchange-correlation functional [J. P. Perdew and A. Zunger, *Phys. Rev. B* **23**, 5048 (1981)] with Troullier-Martins norm conserving pseudopotentials [N. Troullier and J. L. Martins, *Phys. Rev. B* **43**, 1993 (1991)] as implemented in the QUANTUM ESPRESSO code. A kinetic energy cutoff of 55 Ry was used for the wave function. These calculations yielded identical results to the ones using the PBE exchange-correlation functional with ultrasoft pseudopotentials, and were carried out with the only scope of obtaining an input compatible with the Yambo code.
- [22] See Ref. [6] for the nomenclature of the Brillouin zone for the orthorhombic cell used here. The K point of the hexagonal lattice, where the graphene band gap is expected to close at high C concentration, falls between the Γ and Y point within this scheme.
- [23] See Supplemental Material at <http://link.aps.org/supplemental/10.1103/PhysRevLett.108.226805> for the band structure and DFT-RPA optical absorption spectra for the zigzag CBN system, and for supplemental evidence of the dependence of the band gap on C domain size rather than composition.
- [24] X. Zhu and H. Su, *J. Phys. Chem. C* **114**, 17257 (2010).
- [25] T. Olsen, K. W. Jacobsen, and K. S. Thygesen, [arXiv:1107.0600v1](https://arxiv.org/abs/1107.0600v1).
- [26] A. Splendiani, L. Sun, Y. Zhang, T. Li, J. Kim, C.-Y. Chim, G. Galli, and F. Wang, *Nano Lett.* **10**, 1271 (2010).